# Computational simulation of the printing of Newtonian liquid from a trapezoidal cavity

C.A. Powell, M.D. Savage
*Department of Physics and Astronomy, University of Leeds, Leeds, UK*
J.T. Guthrie
*Department of Colour Chemistry, University of Leeds, Leeds, UK*

***Keywords*** *Lagrangian method, Finite element method, Fluid flow*

***Abstract*** *A Lagrangian finite element algorithm is described for solving two-dimensional, time-dependent free surface fluid flows such as those that occur in industrial printing processes. The algorithm is applied using a problem specific structured meshing strategy, implemented with periodic remeshing to control element distortion. The method is benchmarked on the problem of a stretching filament of viscous liquid, which clearly demonstrates the applicability of the approach to flows involving substantial free surface deformation. The model printing problem of the transfer of Newtonian liquid from an upturned trapezoidal trench (3-D cavity with a large transverse aspect ratio) to a horizontal substrate, which is pulled perpendicularly downwards from the cavity, is solved computationally using the Lagrangian scheme. The idealized 2-D liquid motion is tracked from start-up to the point where a thin sheet forms – connecting the liquid remaining in the cavity to a "sessile" drop on the moving substrate. The effect of varying substrate separation speed is briefly discussed and predictions are made for approximate drop volumes and "limiting" domain lengths.*

## 1. Introduction

In a number of industrial printing processes it is necessary to transfer liquids exhibiting various rheologies from engraved cavities to a substrate in order to create a liquid pattern on the latter. For example, in both the coating and printing industries gravure rolls (rolls engraved with tiny cells/cavities) are used extensively for the deposition of liquid onto a web or other surface prior to drying, for the production of a wide range of products including: cartons, packaging systems, plastic films, metal foils and magazine covers. In gravure printing transfer is direct from tiny cells to a substrate wrapped around a soft backing roll – giving rise to a pattern of discrete liquid dots. In gravure coating, however, the liquid transfer mechanism is indirect; liquid, evacuated from the cells by the action of a passing meniscus (Powell *et al.*, 2000), in turn supplies a small coating "bead" from which a continuous film of uniform

International Journal of Numerical Methods for Heat & Fluid Flow, Vol. 12 No. 4, 2002, pp. 338-355.

DOI 10.1108/09615530210433251

The authors wish to thank the Field Group for supporting the research. C. Powell is funded by EPSRC grant GR/M89249.

thickness is coated to the substrate. Recent experimental studies (eg Benkreira and Patel (Benkreira and Patel, 1993)) have done much to further our understanding of the gravure coating process, whilst 2-D finite element (Powell *et al.*, 2000) and 1-D finite difference (Schwartz *et al.*, 1998) simulations of the meniscus-driven evacuation of liquid from individual gravure cavities have further elucidated the process. To date, however, there has been no corresponding numerical modelling of the gravure printing process to accompany experimental studies (Kunz, 1983; Piette *et al.*, 1997; Bohan *et al.*, 2000).

Other common examples of engraved-cavity based printing processes are pad printing (Collard, 1984), where the relevant transfer of link is from a cavity to a pad (or tampon) that is pressed downwards against the cavity and then lifted perpendicularly away, and screen printing (Guthrie, 1992; Mock, 1999), in which ink is flooded over a screen containing open image areas, and a squeegee is then drawn across the screen – simultaneously pushing the screen against a substrate and forcing ink through the open areas. The particular feature of interest to us in screen printing is the reopening of the gap between screen and substrate and the subsequent stretching of liquid from the screen image areas once the squeegee passes. To date there has been no attempt to computationally simulate liquid transfer in either pad or screen printing.

We note that the problem of drop formation from an orifice, of central importance to an understanding of ink-jet printing, has – in contrast to the engraved-cavity based processes mentioned above – received a great deal of attention both experimental and computational. Indeed, a variety of numerical approaches have been adopted to simulate drop formation including volume-of-fluid (VOF) (Zhang, 1999) and an Eulerian finite element method employing a purpose-designed mesh (Wilkes *et al.*, 1999). These different numerical approaches have their relative strengths and weaknesses. The VOF method, for example, does not exhibit a very high degree of accuracy on small scales due to the use of a fixed mesh, though this is compensated for by the fact that meshing and logic problems are removed – enabling straightforward simulation of complicated free surface behaviour.

In the present work we employ of Lagrangian finite element algorithm to solve the 2-D, time-dependent free surface flows, subject to substantial free surface deformation, that typically occur in cavity-based printing processes. Lagrangian finite element analysis is recognised as a very accurate tool for studying the transient free surface fluid flows that occur in a variety of engineering applications, including: thin film coating (Bach and Hassager, 1985), sloshing flows (Ramaswamy *et al.*, 1986), industrial metal casting (Muttin *et al.*, 2001) and wave breaking (Radovitzky and Ortiz, 1998). The major advantage is the use of a convected computational mesh, which enables simple, yet very accurate, tracking of the free surfaces – provided, of course, that at any time a mesh may be generated that discretises the domain effectively. We

employ a problem specific structured meshing strategy to implement the Lagrangian algorithm, together with periodic remeshing to control element distortion. In the next section the method is outlined, with attention drawn to important features, and then in section 3 the method is benchmarked on the problem of a stretching liquid filament. As a first step to understanding the micro-scale liquid transfer processes occurring in cavity-based printing, we formulate and solve numerically an idealised printing problem in which liquid is transferred from an upturned trapezoidal cavity to a moving substrate.

## 2. Lagrangian finite element method

### *2.1 Governing equations*

Denoting a typical velocity by $U$ and a typical length scale by $d$, then the non-dimensional equations of momentum and mass conservation for an incompressible, Newtonian fluid of density $\rho$, viscosity $\mu$ and surface tension $\tau$ are written in Eulerian form as:

$$\mathrm{Re}\left(\frac{\partial \underline{u}}{\partial t} + \underline{u}\cdot\nabla\underline{u}\right) = \nabla\cdot\underline{\underline{\sigma}} + \mathrm{St}\hat{\underline{g}}, \tag{1}$$

$$\nabla\cdot\underline{u} = 0. \tag{2}$$

Here $\underline{u}$ denotes the fluid velocity, $\hat{\underline{g}}$ is a unit vector in the direction of gravity ($g$), $\mathrm{Re} = \rho U d/\mu$ and $\mathrm{St} = \rho g d^2/\mu U$ are the Reynolds and Stokes numbers, and the stress tensor, $\underline{\underline{\sigma}}$, is defined by

$$\underline{\underline{\sigma}} = -p\underline{\underline{I}} + [\nabla\underline{u} + \nabla\underline{u}^T]. \tag{3}$$

We use the Lagrangian description of the flow in which the fluid particle locations, and hence the dependent variables, are functions of some known initial configuration, $\underline{x}_0$ (defined at time $t_0$), and the time elapsed. Thus

$$\underline{x} = \underline{x}(\underline{x}_0, t_0, t), \quad \underline{u} = \underline{u}(\underline{x}_0, t_0, t), \quad p = p(\underline{x}_0, t_0, t). \tag{4}$$

The major advantage of this description is that the computational mesh is identified with the fluid and hence convected with the flow. For free surface simulations this implies that nodes in the computational discretisation that are located on a free surface stay there as the fluid domain evolves, and these nodes are simply found as part of the overall fluid deformation, $\underline{x} = \underline{x}(\underline{x}_0, t_0, t)$. As a consequence the location of moving free surfaces and the imposition of boundary conditions there are rendered straightforward, whereas if one used the alternative Eulerian description of the fluid it would be necessary to impose an additional "kinematic" condition to solve for the free surface nodes, e.g. ref. Wilkes *et al.*, 1999.

*2.2 Boundary conditions*

On no-slip boundaries essential velocity conditions are imposed exactly. Natural free surface conditions are imposed in the standard way (Ruschak, 1980) using the familiar normal stress balance:

$$\hat{\underline{n}} \cdot \underline{\underline{\sigma}} = \frac{1}{\mathrm{Ca}} \frac{\mathrm{d}\hat{\underline{t}}}{\mathrm{d}s}, \tag{5}$$

where $\underline{t}$ and $\hat{n}$ are, respectively, unit vectors tangent and normal to the free surface, $\mathrm{Ca} = \bar{\mu} U/\tau$ is the capillary number, and $s$ denotes length along the free surface.

Determination of the correct mathematical treatment for a contact line, which occurs where a free surface meets a solid boundary under dynamic conditions, is the subject of much theoretical research (see Hocking (1994) and Shikhmurzaev (1997) for two fundamentally different perspectives on the problem). In terms of incorporating a contact line into a finite element simulation of flow involving capillary effects, the two key issues that must be resolved are:

(1) the introduction of local tangential slip near the contact line to remove the stress singularity that occurs if the usual no-slip conditions are applied (Dussan, 1976),

(2) the boundary condition at the contact line relating the contact angle to the independent variables and physical parameters.

In addition a degree of local mesh refinement is required to incorporate the modeling and accurately resolve the high velocity gradients. A recent paper (Powell and Savage, 2001) gives the specific numerical details of how this may be accomplished for the particular choice of a "Tanner law" (Greenspan, 1978) boundary condition, relating contact angle to contact line speed. An identical treatment is used for incorporating the moving contact lines in the printing application presented in this work. The only difference here is the choice of a constant dynamic contact angle boundary condition, which is imposed by satisfying the following equation:

$$\hat{\underline{t}}_b \cdot \hat{\underline{t}}_{fs} = \cos \theta_{\mathrm{D}}, \tag{6}$$

where $\theta_{\mathrm{D}}$ is the prescribed dynamic contact angle, $\hat{t}_b$ is the known tangent to the solid boundary and $\hat{\underline{t}}_{fs}$ is the free surface tangent at the contact line, which may be calculated accurately using the isoparametric element representation. This equation allows the contact line location to be updated as part of the overall numerical solution scheme.

*2.3 Finite element implementation*

The Lagrangian finite element algorithm used to solve the governing equations, subject to appropriate initial and boundary conditions, has been

described elsewhere (Powell and Savage, 2001), thus here we only given an outline. The fluid domain is discretised using isoparametric triangular V6/P3 elements (Zienkiewicz, 1977; Taylor and Hood, 1973), so the velocity components and pressure are interpolated over an element as:

$$u = \sum_{i=1}^{6} N_i(x,y)\bar{u}_i(t), \quad v = \sum_{i=1}^{6} N_i(x,y)\bar{v}_i(t), \quad p = \sum_{i=1}^{3} L_i(x,y)\bar{p}_i(t), \tag{7}$$

where "–" denotes a nodal value. We apply the Galerkin method to obtain the finite element equations:

$$[M]\begin{pmatrix} \dot{\underline{U}} \\ \dot{\underline{V}} \\ \dot{P} \end{pmatrix} + [C]\begin{pmatrix} \underline{U} \\ \underline{V} \\ \underline{P} \end{pmatrix} = (F), \tag{8}$$

where $\underline{U} = (\bar{u}_1, \ldots, \bar{u}_6), \underline{V} = (\bar{v}_1, \ldots, \bar{v}_6), \underline{P} = (\bar{p}_1, \bar{p}_2, \bar{p}_3)$ and "$\cdot$" denotes the material time derivative $D/Dt$. The matrix $M$ is the mass, or inertia matrix, $C$ is the diffusion matrix and $F$ contains the gravity and surface tension contributions [1]. For a given set of element coordinates the matrices $M$, $C$ and $F$ may be evaluated using numerical integration; here all domain integrals are approximated using a 4-point Gaussian scheme and boundary integrals using a 3-point scheme. For time integration we employ a "$\Theta$-scheme":

$$\begin{pmatrix} \underline{U} \\ \underline{V} \\ \underline{P} \end{pmatrix}_{t+\Delta t} = \begin{pmatrix} \underline{U} \\ \underline{V} \\ \underline{P} \end{pmatrix}_{t} + \Delta t \left[ \Theta \begin{pmatrix} \dot{\underline{U}} \\ \dot{\underline{V}} \\ \dot{P} \end{pmatrix}_{t+\Delta t} + (1-\Theta) \begin{pmatrix} \dot{\underline{U}} \\ \dot{\underline{V}} \\ \dot{\underline{P}} \end{pmatrix}_{t} \right] \tag{9}$$

$\Theta$ is initially given the value 1, corresponding to a simple backward difference approximation, then subsequently $\Theta$ takes a value of 1/2 – thus switching to the second-order accurate Crank-Nicolson, or trapezoidal, method. This switching strategy avoids the need for specifying initial conditions on pressure. In a previous study of surface tension dominated flows (Powell and Savage, 2001) it was noted that changing $\Theta$ to 1/2 too quickly can introduce significant inaccuracies into the solution, thus in such flows the switching is delayed for several time steps. A value for $\Delta t$ is found heuristically by testing several different time steps and comparing the solutions.

The iterative solution scheme, used to advance the fluid motion through a time increment $\Delta t$ and obtain the new fluid domain and velocity and pressure fields, is as follows (see refs Bach and Hassager (1985) and Powell and Savage (2001) for further information):

(1) Make initial estimates of velocities and coordinates at time $t + \Delta t$:

$$\underline{u}^1_{t+\Delta t} = \underline{u}_t, \quad \underline{x}^1_{t+\Delta t} = \begin{cases} \underline{x}_t + \Delta t \underline{u}^1_{t+\Delta t} & \text{tstep} = 1 \\ \underline{x}_t + \frac{\Delta t}{2}(\underline{u}^*_{t+\Delta t} + \underline{u}^1_{t+\Delta t}) & \text{tstep} > 1 \end{cases} \tag{10}$$

where tstep is the number of the current time step and $\underline{u}^*_{t+\Delta t}$ is given by a two step Adams-Bashforth estimate:

$$\underline{u}^*_{t+\Delta t} = \underline{u}_t + \frac{\Delta t}{2}\left[3\frac{D\underline{u}_t}{Dt} - \frac{D\underline{u}_{t-\Delta t}}{Dt}\right]. \tag{11}$$

Then starting with $n = 1$ repeat steps (2)–(4).

(2) Assemble the element equations on configuration $\underline{x}^n_{t+\Delta t}$, impose boundary conditions and solve to find $\underline{u}^{n+1}_{t+\Delta t}$ and $p^{n+1}_{t+\Delta t}$; the large system of linear finite element equations is solved by Gaussian elimination using Hood's frontal method (Hood, 1976).

(3) Find a new configuration from:

$$\underline{x}^{n+1}_{t+\Delta t} = \underline{x}_t + \frac{\Delta t}{2}\left(\underline{u}^{n+1}_{t+\Delta t} + \underline{u}_t\right). \tag{12}$$

(4) Check for convergence by seeing if $\underline{x}^{n+1}_{t+\Delta t} - \underline{x}^n_{t+\Delta t}$ is less than some specified tolerance; if not repeat from step (2).

Steps (1)–(4) are repeated until the preassigned total time is reached, or the simulation reaches steady state.

*2.4 Meshing issues*

At the end of each time step the amount of mesh deformation is calculated using the following measure (Bach and Hassager, 1985):

$$D_p = \frac{V_p}{\min_n N \; J_n W_n}, \tag{13}$$

where $J_n$ is the determinant of the transformation Jacobian from local to global coordinates at the $n$th Gauss point in element $p$, $W_n$ is the Gaussian weight for the $n$th Gauss point, $N$ is the number of Gauss points and $V_p = \sum_{i=1}^{N} J_i W_i$ is the element area. $D_p$ takes its minimum value of 1.0 when element $p$ is undeformed, but this value grows as the element distorts (becoming infinite if the Jacobian becomes singular). Our numerical algorithm searches through each element of the mesh and checks that $D_p$ is less than some maximum permitted tolerance, if $D_p$ exceeds this limit in one or more elements the decision is made to remesh.

In a previous application of the present Lagrangian scheme to capillary flow involving dynamic contact line motion (Powell and Savage, 2001) the free

surface deformations are not particularly significant and hence the construction of a structured mesh is not difficult and few remeshings are required to prevent element distortion. Printing problems, by contrast, typically involve liquid domains that are subject to severe free surface deformations thus in order to apply the Lagrangian scheme it is necessary to either devise more flexible problem specific structured meshes or resort to a fully automatic unstructured mesh approach. We adopt the former alternative, and so the fluid domain is initially discretised and then periodically remeshed using structured meshes of isoparametric triangular V6/P3 elements.

It is worth noting that a great deal of research has been carried out into the development of unstructured mesh generation and adaptive refinement algorithms, see, for instance, refs Shephard (1988); Joe (1991); Rebay (1993). Significant advances in these fields have undoubtably increased the attractions of Lagrangian finite element analysis to CFD practitioners, since early Lagrangian-based algorithms were carried out on fixed meshes and could not cope with large fluid domain deformations. Indeed, in recent years unstructured meshing algorithms have been incorporated into Lagrangian finite element simulators in studies of metal casting (Muttin *et al.*, 1993) and wave breaking (Radovitzky and Ortiz, 1998). However aspects of any fluid domain meshing procedure invariably remain problem specific, since the design of a computational mesh represents both a physical as well as a geometrical problem. Hence adding mesh refinement for special features such as moving contact lines and sharp boundary corners often requires non-trivial user interaction even for an unstructured algorithm. Furthermore, serious programming issues are encountered when an unstructured mesh is used in conjunction with a highly efficient frontal solution approach such as Hood's method (Hood, 1976) which we employ in this study. The task of renumbering elements and nodes in order to minimize the frontwidth becomes far from straightforward, and the numbering scheme must be recalculated every time the mesh is updated. For these reasons in this work we follow the structured mesh route; details about the mesh structure used for a specific problem are given in the appropriate place.

Once the new mesh is generated accurate mesh-to-mesh transfer is ensured by iteratively solving the old element interpolation equations to locate nodes in the new mesh and then employing the isoparametric mapping (Bach and Villadsen, 1984). When this is completed the simulation may continue through another time increment.

## 3. Validation and applications

### *3.1 Stretching viscous filament*

We consider a stretching (planar) viscous filament, as illustrated in Figure 1. A quantity of viscous liquid is initially held between two stationary plates, the top plate is then impulsively pulled perpendicularly away from the bottom

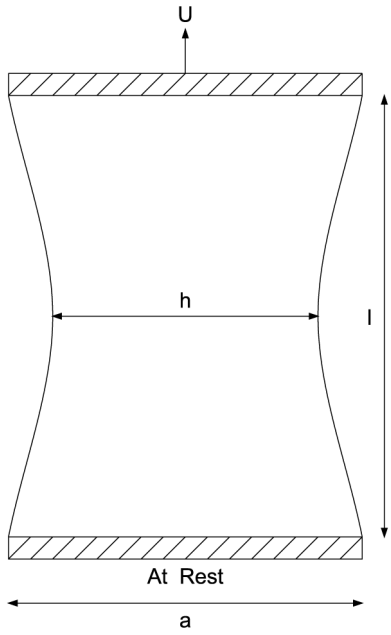


**Figure 1.**
The stretching of a (planar) viscous fluid filament

plate with a constant velocity $U$. Perfect adherence is assumed between the liquid and the plates and consequently the filament thins most in its central region. Stretching filament devices are used in experiments to test the extensional properties of polymers, and numerical simulations of viscoelastic fluids often use the stretching filament as a benchmark problem, eg Harlen, (1996). In the present study inertia effects are assumed to be small ($\mathrm{Re} = \rho Ua/\mu$ is given a value of $10^{-2}$), furthermore, gravity, which serves to create a top-bottom asymmetry in the filament, and surface tension, which causes an extra squeezing effect in the middle of the filament, are both neglected. On the plates two no-slip velocity boundary conditions are specified, and the free surface normal stress balance reduces to:

$$\hat{\underline{n}} \cdot \underline{\underline{\sigma}} = \underline{0}. \tag{14}$$

For simplicity the fluid filament is assumed to have an initially square shape (with $l/a = 1.0$), Figure 2 shows the initial finite element mesh containing 200 elements. As the simulation proceeds and the filament stretches the number of horizontal element strips is increased automatically during remeshing so that the free surface representation retains a specified level of refinement. Nodes are equally spaced along the free surfaces, resulting in more element strips in the regions of high curvature adjacent to the plates. Figure 3 shows the finite element mesh and the velocity vectors when the aspect ratio is 3.5 and the fluid

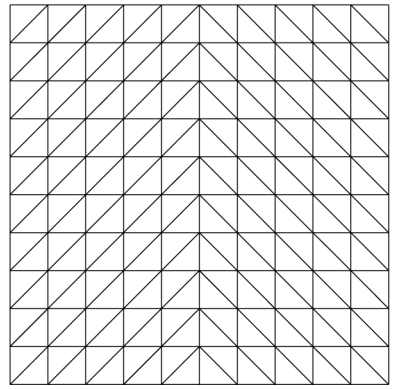

**Figure 2.**
Initial finite element mesh

has undergone considerable deformation; the simulation can be continued without difficulty until the filament becomes very thin and problems of mesh resolution are eventually encountered. The mesh shown contains 416 elements – more than double the initial number. The calculated change in volume for this simulation is negligible, and the filament is found to be top-bottom symmetric as predicted in the absence of gravity.

The velocity vectors shown in Figure 3(b) are scaled with respect to the speed of the top plate; the fluid motion is essentially unidirectional and the velocities increase linearly with length along the filament.

Figure 4 gives the minimum filament thickness, $h_{min}$, as a function of time – quantities being non-dimensionalised using $a$ and $U$ as typical scales. Initially $h_{min}$ decreases quite rapidly but the rate of thinning gradually slows. One may obtain a simple analytical expression for the evolving free surface position by assuming that the filament thickness is approximately constant except in the regions very close to the plates (as suggested by Figure 3). In this case we assume $h$ is independent of length along the filament, i.e. $h = h(t)$, then conservation of mass yields the following:

$$h\frac{\partial u}{\partial x} + \frac{\mathrm{d}h}{\mathrm{d}t} = 0, \tag{15}$$

where the velocity $u$ is a function of length along the filament, $x$, and time. Taking the plate velocities as approximate conditions on $u$, imposed at some unspecified positions "close to the plates", and taking the initially square domain shape as an initial condition on $h$, the above equation may be integrated to give

$$h = \frac{1}{1+t}. \tag{16}$$

This expression is also plotted in Figure 4 where happily the agreement for the sheet thinning between the simple analytical (ANAL) and numerical (FEM)

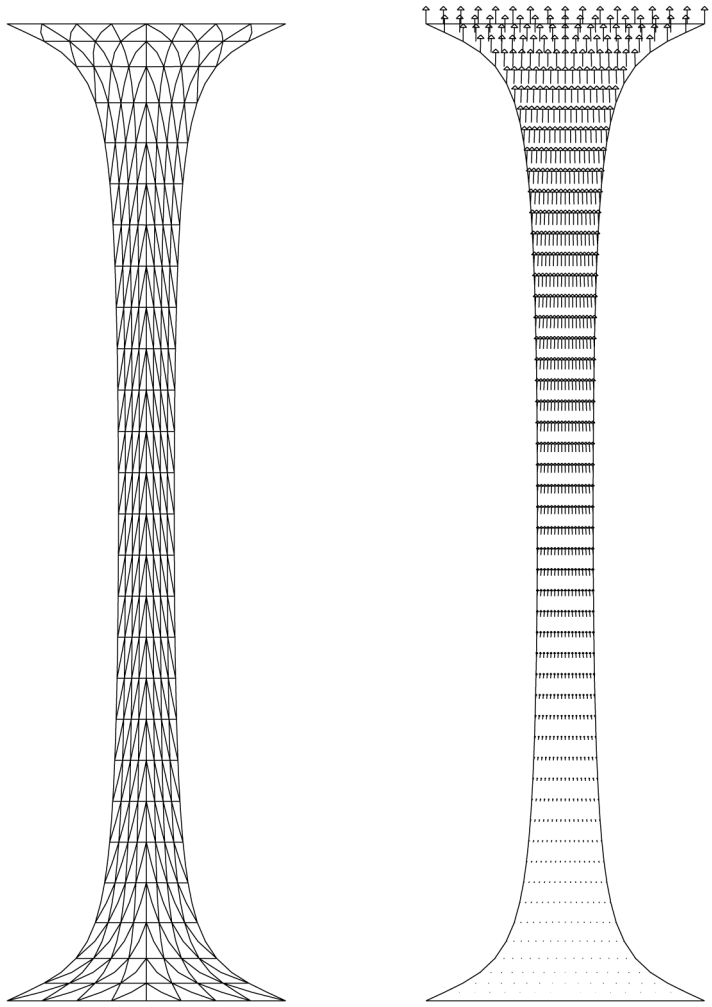


**Figure 3.**
Result of filament stretching simulation when $l/a = 3.5$: (a) finite element mesh, (b) velocity vectors

curves is pretty close. Of course, the difference between the two curves occurs because the simple analytical model takes no account of the regions of high meniscus curvature at the plates and hence cannot predict the sheet thinning exactly.

*3.2 Printing liquid from a trapezoidal cavity*

Here the Lagrangian finite element algorithm is employed to simulate the idealized 2-D transfer process, involving a Newtonian fluid pulled from an upturned trapezoidal trench (which may be thought of as a 3-D cavity with a large transverse aspect ratio) by a downwards moving substrate. The

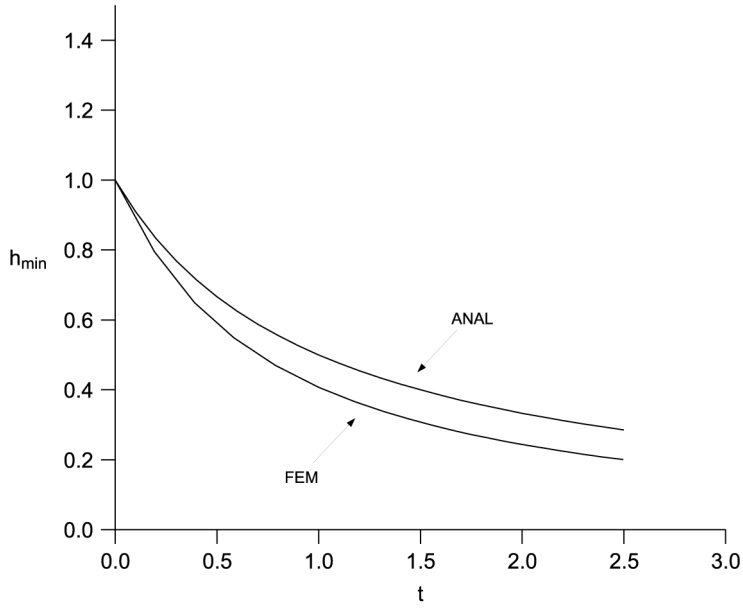


**Figure 4.**
The minimum filament thickness as a function of time calculated numerically (FEM); also plotted is the approximate analytical expression $h_{\min} = 1/1 + t$ (ANAL)

trapezoidal design is commonly used in printing industries and so has been chosen as a representative cavity for this problem. In our model (see Figure 5) we initially assume the presence beneath the cavity of a liquid layer bounded by two vertical free surfaces to overcome the significant theoretical difficulties that are introduced if the cavity and substrate are initially in contact. The lower surface is impulsively pulled downwards with constant speed $U$ and the liquid is set in motion subject to the following assumptions:

(1) There is perfect adherence between the liquid and the moving surface on which there are two "static" contact lines. In real applications there will possibly be some amount of slippage between liquid and solid at the

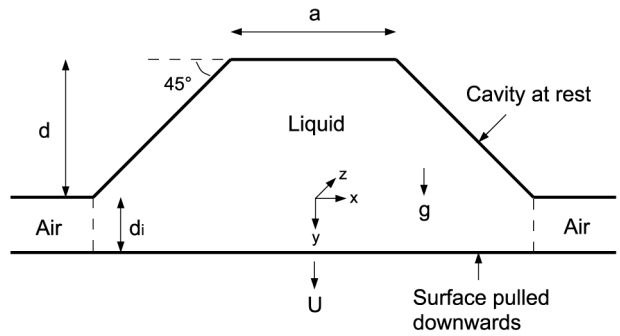


**Figure 5.**
Cross-section of the trapezoidal trench at $t = 0$.

contact lines, though in practice substrates are suitably prepared so that the printed liquids tend to adhere to them.

(2) Here exists local slip between the liquid and the trapezoidal cavity walls at two dynamic contact lines – the specific modelling of which is discussed below.

(3) Away from the edges of the trench the liquid motion is approximately independent of the transverse coordinate $z$, up to the time when a thin viscous sheet is formed, connecting liquid remaining in the trench to that on the downward moving surface. The computation is terminated when the minimum sheet thickness falls below a specified tolerance, prior to which it is assumed that the influence of transverse edge effects and the formation of instabilities can both be ignored within the main body of the sheet.

Taking the speed of the lower surface, $U$, and the cavity depth, $d$, as typical scales, then for a Newtonian fluid with viscosity $\mu$, density $\rho$ and surface tension $\tau$, non-dimensionalising the problem introduces the following groups: $\mathrm{Re} = \rho U d/\mu$, $\mathrm{Ca} = \mu U/\tau$, and $\mathrm{St} = \rho g d^2/\mu U$. To incorporate the dynamic contact lines we specify:

(1) an explicit linear slip velocity distribution, introducing an unknown slip length, $l$, which must be estimated;

(2) a constant dynamic contact angle, $\theta_D$ (measured through the fluid).

Thus the contact lines are allowed to move along the sloped cavity walls, though they are assumed to re-pin if they reach the bottom corners of the cavity. There are, of course, a variety of possibilities for the dynamic contact line treatment. In the absence of any experimental visualisations of micro-scale cell emptying in printing processes we chose a straightforward constant angle model, though it would not be difficult to refine the modeling in light of experimental input at a later time (see Powell and Savage, (2001) for example).

Figure 6 shows the evolving liquid domain for a sample calculation in which the following parameter values were used: $a/d = 1.0$, $\mathrm{St} = 0.1$, $\mathrm{Ca} = 0.1$, $\mathrm{Re} = 1.0$, $\theta_D = 75°$. In the early stages of the motion the menisci become highly curved and the effect of surface tension appears to dominate. As the liquid domain extends the gravitational acceleration has more of an effect, the liquid being forced downwards out of the cavity and into the sheet. In the later stages of the simulation a thin liquid sheet forms, connecting the fluid that remains in the cavity to a "sessile" drop forming on the moving surface. In this calculation the contact lines do in fact reach the base of the cavity where it is assumed that they re-pin. The simulation is terminated when the minimum sheet thickness falls below 0.1, this is an arbitrary stopping point when it is possible to obtain an estimate of the fraction of the initial liquid in the large sessile drop by calculating the fraction below the minimum sheet (or "neck")

location – though it should be noted that the algorithm may in fact be continued without trouble until the sheet is much thinner. For this sample calculation approximately 93 per cent of the liquid lies below the neck when the simulation is terminated.

Two snapshots of the computational mesh and velocity vectors, taken at times $t = 0.072$ and $t = 2.3$, are shown in Figure 7. The mesh pictures illustrate how a structured strategy using horizontal strips of elements is able to effectively discretise the liquid domain from start-up through to the later stages of the motion. Local mesh refinement is included in the dynamic contact line regions in order to accurately resolve the velocity field. At $t = 2.3$, when the contact lines have re-pinned at the cavity base and the rounded sessile drop is well formed, the mesh shown is constructed by equally spacing the nodes along the free surface. This naturally results in a greater number of element strips in the regions of rapidly changing velocity adjacent to the cavity base and where the sheet opens out into the sessile drop. Furthermore, since each horizontal element strip contains the same number of elements, we achieve a much higher mesh refinement in the thin sheet region. The corresponding velocity plot at $t = 2.3$ shows that gravity is indeed the dominant effect in the later stages of the simulation, with the highest velocities generated as fluid is forced downwards through the neck region and into the drop. We note that simulations are restricted to cases where $\theta_D$ is strictly greater than 45°, since the use of horizontal element strips in the discretisation cannot cope with free surfaces that become multi-valued functions of the vertical coordinate, $y$. Of course, if subsequent visualization experiments point to much smaller values of the contact angle then a modified, more general meshing strategy can be

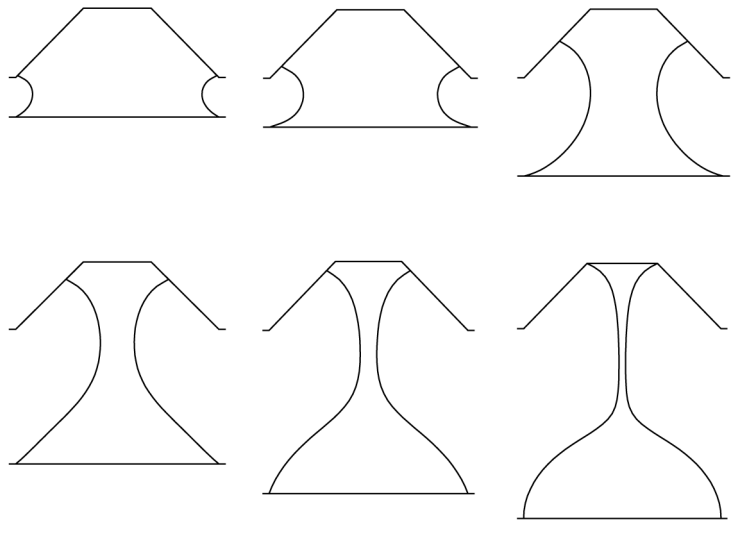

**Figure 6.**
Result of simulation performed with the following parameters: $a/d = 1.0$, $\theta_D = 75°$, $\mathrm{Re} = 1.0$, $\mathrm{Ca} = 0.1$, $\mathrm{St} = 0.1$; the evolving liquid domain is shown at six different times: $t = 0.072$, 0.215, 0.931, 1.498, 1.868, 2.3

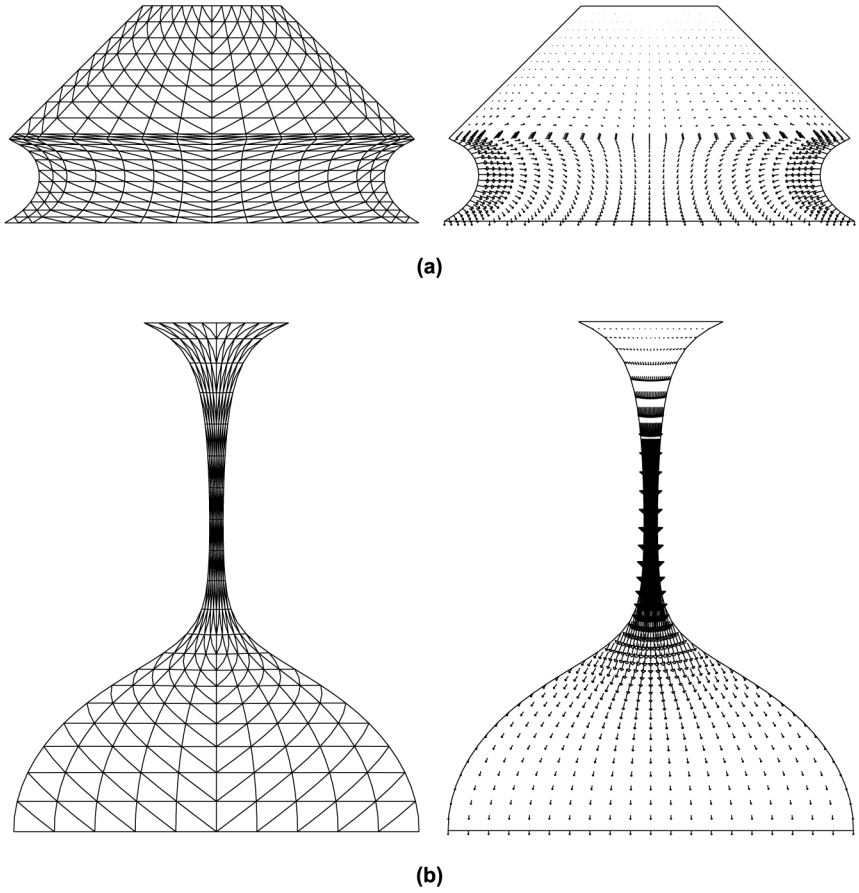


**Figure 7.**
Computational mesh and velocity vectors shown at times (a) $t = 0.072$ and (b) $t = 2.3$

implemented into the Lagrangian algorithm. Mesh resolution studies have been conducted to determine levels of refinement resulting in mesh independent results; at the point when a simulation is terminated a suitable mesh typically contains around 600 elements.

Figure 8 shows the minimum sheet thickness as a function of time for the same simulation. In the early stages of the liquid motion the rate of domain thinning is large, but this rate gradually slows as the sheet forms and continues to stretch. It is not possible to determine if the thin sheet is close to rupture since there is no large negative gradient on the curve; indeed this suggests that at later times any sheet rupture will be three-dimensional in nature.

To demonstrate the predictive use of our algorithm to industrialists and experimentalists seeking to control their liquid transfer process, the effect of varying the separation speed of the substrate is explored. Denoting a reference

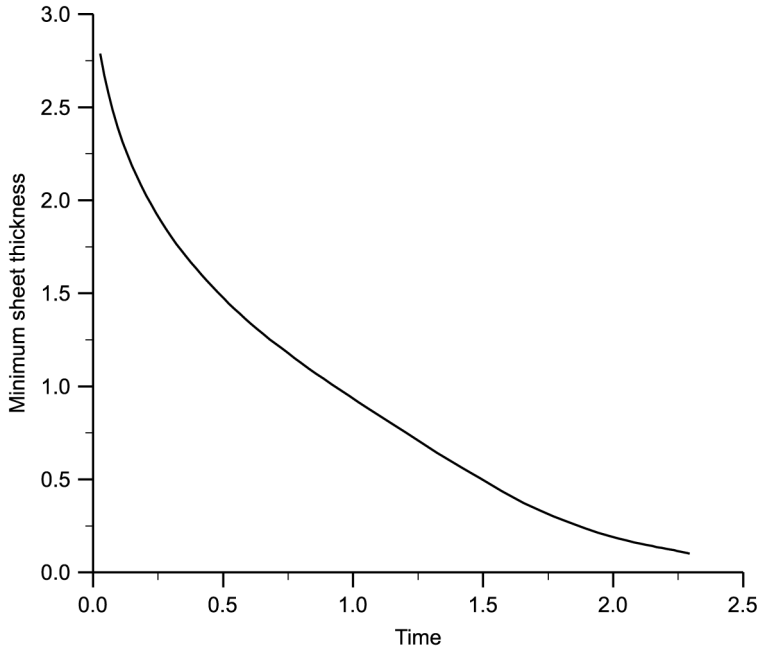


**Figure 8.**
Minimum sheet thickness versus time for the sample calculation

substrate speed by $U^*$ which gives Reynolds, Stokes and capillary numbers (Re*, St*, Ca*) say, then changing the speed to $U = nU^*$ changes the dimensionless groups to ($n$Re*, St*/$n$, $nCa^*$). Here it is assumed that $U^*$ leads to the following group values: Re* = 1.0, St* = 0.1 and Ca* = 0.1 (with $a/d = 1.0$ and $\theta_D = 75°$), and the effects of halving and doubling the separation speed by taking $n$ equal to 0.5 and 2, respectively, are considered. It is immediately clear from Figure 9(a), which compares liquid domains when the minimum sheet thickness falls below 0.1, that increasing $U/U^*$ from 0.5 to 2.0 leads to:

- a significant lengthening of the "final" fluid domain,
- a longer thin sheet region and
- a corresponding decrease in the fraction of liquid in the sessile drop.

These trends are quantified in Figures 9(b), which plots the final distance from cavity to substrate, and 9(c), which gives the fraction of liquid lying below the neck. The shortest limiting domain length and largest sessile drop fraction (when approximately 94 per cent of the liquid lies below the neck) occur at the lowest separation speed, which is in accord with intuition since the gravity-driven cavity emptying has more time to occur than at a higher substrate speed. This suggests that one may control the approximate sessile drop size to a certain extent by simply varying the substrate speed, but a high speeds the creation of a long thin sheet prior to rupture may be an undesirable side-effect.

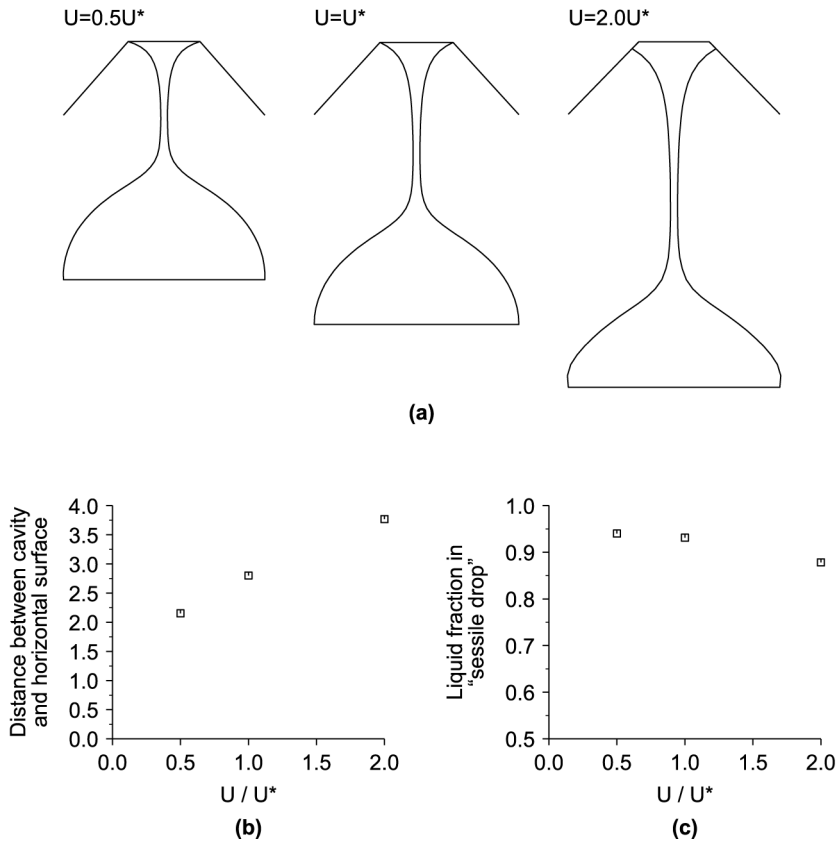


**Figure 9.**
The effect of $U/U^*$ upon the cavity emptying process ($U^*$ denoting a reference substrate speed – see text): (a) "final" liquid domain profiles, (b) "final" distance from top of cavity to moving substrate, (c) approximate final liquid fraction in "sessile drop"

## 4. Conclusion

A Lagrangian finite element algorithm for solving time-dependent free surface flows, which uses a structured meshing strategy to allow for large free surface deformations, has been described and successfully applied to both a stretching filament and a model printing problem. We stress that the cavity emptying work presented here constitutes a first step towards simulating and understanding the (fully three-dimensional) micro-scale liquid transfer phenomena occurring in a range of industrial printing processes. Numerous extensions to the present work are underway, including:

- introduction of an asymmetric separation between the cavity and substrate to account for a roll-based printing configuration such as gravure printing
- incorporation of non-Newtonian rheology to model more realistically the types of inks used in printing processes

- consideration of process instabilities that occur due to imperfect cell filling prior to printing.

An experimental program into the micro-scale printing of liquid from engraved cells under different conditions is currently underway at the University of Leeds. It is intended to report some of the experimental results together with complementary numerical simulations in a future publication.

**Note**

1. Details of the individual contributions to the matrices $M$, $C$ and $F$ are given in numerous papers, see, for example, ref (Bach and Villadsen, 1984).

**References**

Bach, P. and Hassager, O. (1985), "An algorithm for the use of the Lagrangian specification in Newtonian fluid mechanics and applications to free-surface flow", *J. Fluid Mech.*, 152, pp. 173-90.

Bach, P. and Villadsen, J. (1984), "Simulation of the vertical flow of a thin, wavy film using a finite-element method", *Int. J. Heat Mass Transfer*, 27 No. 6, pp. 815-27.

Benkreira, H. and Patel, R. (1993), "Direct gravure roll coating", *Chem. Eng. Sci.*, 48, pp. 2329-35.

Bohan, M.F.J., Claypole, T.C. and Gethin, D.T. (2000), "The effect of process parameters on product quality of rotogravure printing", *Proc. Inst. Mech. Eng. Part B.*, 214 No. 3, pp. 205-19.

Collard, G. (1984), "Pad-transfer printing – taking a new look", *Plastics Engineering*, 40 No. 2, pp. 49-50.

Dussan, V.E.B. (1976), "The moving contact line: the slip boundary condition", *J. Fluid Mech.*, 77 No. 4, pp. 665-84.

Greenspan, H.P. (1978), "On the motion of a small viscous droplet that wets a surface", *J. Fluid Mech.*, 84 No. 1, pp. 125-43.

Guthrie, J.T. (1992), "The physical-chemical and philosophical aspects of screen printing processes", *JOCCA-Surface Coatings International*, 75 No. 3, pp. 94-6.

Harlen, O.G. (1996), "Simulation of viscoelastic flows", in, *First European Coating Symposium On The Mechanics Of Thin Film Coatings*, World Scientific, Singapore pp. 366-74.

Hocking, L.M. (1994), "The spreading of drops with intermolecular forces", *Phys. Fluids*, 6, pp. 3224-8.

Hood, P. (1976), "Frontal solution program for unsymmetric matrices", *Int. J. Numer. Meth. Engng.*, 10, pp. 379-99.

Joe, B. (1991), "GEOMPACK – a software package for the generation of meshes using geometric algorithms", *Adv. Eng. Software*, 13 No. 5–6, pp. 325-31.

Kunz, W. (1983), "Interactions between materials involved in gravure printing", *Wochenblatt Fur Papierfabrikation*, 111 No. 6, pp. 1922-2.

Mock, G.N. (1999), "The development of rotary-screen printing", *Textile Chemist and Colorist & American Dyestuff Reporter*, 1 No. 3, pp. 43-9.

Muttin, F., Coupez, T., Bellet, M. and Chenot, J.L. (1993), "Lagrangian finite element analysis of time-dependent viscous free-surface flow using an automatic remeshing technique: application to metal casting flow", *Int. J. Numer. Meth. Engng.*, 36, pp. 2001-15.

Powell, C.A. and Savage, M.D. (2001), "Numerical simulation of transient free surface flow with moving contact lines", *Commun. Numer. Meth. Engng.*, 17, pp. 581-8.

Piette, P., Morin, V. and Maume, J.P. (1997), "Industrial-scale rotogravure printing tests", *Wochenblatt Fur Papierfabrikation*, 125 No. 16, pp. 744.

Powell, C.A., Savage, M.D. and Gaskell, P.H. (2000), "Modelling the meniscus evacuation problem in direct gravure coating", *Trans. Inst. Chem. Eng.*, 78 No. A, pp. 61-7.

Rebay, S. (1993), "Efficient unstructured mesh generation by means of Delaunay triangulation and Bowyer-Watson algorithm", *J. Compute. Phys.*, 105, pp. 125-38.

Ruschak, K.J. (1980), "A method for incorporating free boundaries with surface tension in finite element fluid flow simulators", *Int. J. Numer. Meth. Engng.*, 15, pp. 639-48.

Radovitzky, R. and Ortiz, M. (1998), "Lagrangian finite element analysis of Newtonian fluid flows", *Int. J. Numer. Meth. Engng.*, 43, pp. 607-19.

Ramaswamy, B., Kawahara, M. and Nakayama, T. (1986), "Lagrangian finite element method for the analysis of two-dimensional sloshing problems", *Int. J. Numer. Meth. Fluids*, 6, pp. 659-70.

Shephard, M.S. (1988), "Approaches to the automatic generation and control of finite element meshes", *Appl. Mech. Rev.*, 41 No. 4, pp. 169-85.

Shikhmurzaev, Y.D. (1997), "Moving contact lines in liquid/liquid/solid systems", *J. Fluid Mech.*, 334, pp. 211-49.

Schwartz, L.W., Moussalli, P., Campbell, P. and Eley, R.R. (1998), "Numerical modeling of liquid withdrawal from gravure cavities in coating operations", *Trans. Inst. Chem. Eng.*, 76 No. A, pp. 22-9.

Taylor, C. and Hood, P. (1973), "A numerical solution of the Navier-Stokes equations using the finite element technique", *Computers and Fluids*, 1, pp. 73-100.

Wilkes, E.D., Phillips, S.D. and Basaran, O.A. (1999), "Computational and experimental analysis of dynamics of drop formation", *Phys. Fluids*, 11 No. 12, pp. 3577-98.

Zhang, X. (1999), "Dynamics of drop formation in viscous flows", *Chem. Eng. Sci.*, 54, pp. 1759-74.

Zienkiewicz, O.C. (1977), *The finite element method*, McGraw-Hill.